JACS
JOURNAL OF THE AMERICAN CHEMICAL SOCIETY
Article
pubs.acs.org/JACS

Specific Material Recognition by Small Peptides Mediated by the Interfacial Solvent Structure

Julian Schneider[†] and Lucio Colombi Ciacchi*[,†,‡]

[†]Hybrid Materials Interfaces Group, Faculty of Production Engineering and Bremen Center for Computational Materials Science, University of Bremen, D-28359 Bremen, Germany

[‡]Fraunhofer Institute for Manufacturing Technology and Applied Materials Research IFAM, D-28359 Bremen, Germany

Supporting Information

ABSTRACT: We present evidence that specific material recognition by small peptides is governed by local solvent density variations at solid/liquid interfaces, sensed by the side-chain residues with atomic-scale precision. In particular, we unveil the origin of the selectivity of the binding motif RKLPDA for Ti over Si using a combination of metadynamics and steered molecular dynamics simulations, obtaining adsorption free energies and adhesion forces in quantitative agreement with corresponding experiments. For an accurate description, we employ realistic models of the natively oxidized surfaces which go beyond the commonly used perfect crystal surfaces. These results have profound implications for nanotechnology and materials science applications, offering a previously missing structure−function relationship for the rational design of materials-selective peptide sequences.

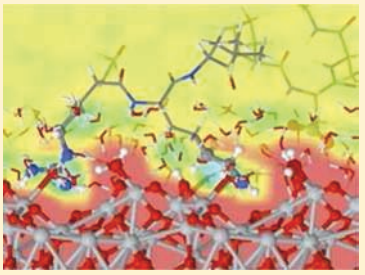

INTRODUCTION

The specific recognition of materials surfaces by small peptide sequences has become a widely investigated, interdisciplinary research topic with fields of application ranging from nanoelectronics to medicine and pharmacology.[1,2] However, a rationalization of the binding driving forces in terms of clear structure−function relationships is missing,[3] as the atomistic details of material surfaces in a wet environment are hard to elucidate both experimentally and theoretically.[4−7] Even for the case of well-established peptide-materials couples such as the titanium-binding motif minTBP-1, consisting of the amino acid sequence RKLPDA, the mechanisms of interaction remain speculative and based purely on electrostatic arguments.[8−11] Biological recognition, however, is based on a complex interplay of interactions that provide optimal host−guest matching via steric exclusions, hydrophobic/hydrophilic patterns, directional hydrogen bonding, solvent structuring, as well as electrostatics. In fact, a recent molecular dynamics study has pointed out that not only direct surface−molecule interactions, but indirect, solvent-mediated effects govern the adsorption behavior of the RKLPDA peptide on the neutral TiO_2(110) rutile surface.[12] In the present work we unveil the reasons for the bindind selectivity of RKLPDA to Ti against Si using realistic models of their surfaces in an oxidizing, aqueous environment, as constructed from quantitatively accurate first-principles and classical molecular dynamics simulations. We present compelling evidence that the surface-binding specificity of peptides does not originate primarily from a matching of favorable electrostatic interactions but from the ability of amino acid side chains to "sense" the molecular solvent structure at the solid/liquid interface with atomic-scale precision, in a mechanism reminiscent of the "lock-and-key" recognition that characterizes naturally evolved biological systems.

The strong, specific adsorption of peptides to inorganic surfaces has been exploited as an alternative to more expensive and involved covalent immobilization techniques to impart materials a biological functionality,[13] such as enhanced cell growth or antifouling effects.[14,15] Recently, a large variety of amino acid sequences have been identified, which are selective to certain material classes,[2] certain compounds, or even certain crystallographic facets of the same material. In this letter, we will focus mainly on titanium as an ubiquitous implant material whose cell adhesion properties could be enhanced via biofunctionalization.[16−18] A few amino acid sequences exhibiting a characteristic and strong adhesion to Ti have been identified using phage-display techniques.[8,14,19] Among these, the minimum titanium-binding motif minTBP-1 with sequence RKLPDA is probably the most prominent example, as it strongly binds to titanium but not to other metals, such as, for example, iron, chromium, gold, and platinum,[9] nor to organic SAM surfaces.[11] Useful insights into the dependence of the adhesion strength on the single amino acids composing the peptide have been obtained by means of atomic force microscopy (AFM), quartz crystal microbalance (QCM), and, in a single study limited to crystalline rutile, molecular dynamics (MD) techniques.[9−12] The adhesion strength, as measured, for instance, with AFM force spectroscopy, has been found to be strongly decreased upon amino acid mutation, especially of the positively charged R and K residues and of the cyclic P residue, as well as on changing of the residue positions

Received: November 15, 2011
Published: December 23, 2011

   dx.doi.org/10.1021/ja210744g | J. Am. Chem.Soc. 2012, 134, 2407−2413

within the sequence. Since the same peptide binds also, but less strongly, to silicon, the latter surface has often been used as a comparison, as subtle differences in the binding under different conditions may help elucidate the origin of its specific binding mechanism to Ti.[11] This is the subject of our investigations, which go beyond idealized, crystalline surfaces and make use, instead, of realistic surface models of the natively oxidized Ti and Si surfaces in contact with liquid water.

MODELS AND SIMULATION DETAILS

Our surface models have been obtained through extensive first-principles MD simulations of the oxidation and hydration reactions at Si[20−22] and Ti[23,24] surfaces. The interaction of these surfaces with the RKLPDA dissolved in water is described classically, by the force fields developed in ref 24 for the Ti surface and in ref 21 for the Si surface. The protonation state of the surfaces is adjusted to obtain a distribution and density of surface net charges reflecting the experimental conditions of neutral pH and low ionic strength, and the force fields (in particular the atomic point charges) are modified ad hoc on the basis of reference DFT calculations (see Supporting Information). Namely, for Ti (isoelectric point, IEP, between 5.0 and 6.0[25−27]), we introduce both deprotonated $TiOH^-$ and protonated Ti_2OH^+ sites in the ratio of 16:5, which leads to a surface charge density of −0.123 C/m^2, consistent with typical experimental values at neutral pH.[28] For Si (IEP of 3.0 or lower[27,29]), we introduce exclusively negative SiO^- sites by deprotonation of terminal hydroxyl groups in order to achieve a surface charge density of −0.136 C/m^2.[30]

The RKLPDA peptide is described by the AMBER force field.[31] Its termini are capped by ACE (i.e CH_3CO-) and NME (i.e., $-NHCH_3$) residues to avoid charged end groups that are not present in the experimentally studied molecules.[10,11]

The adsorption of the RKLPDA peptide is studied via extensive classical MD simulations performed using the LAMMPS[32] MD package with explicit TIP3P[33] water molecules under periodic boundary conditions. To increase the computational efficiency, the surface atoms except for hydroxyl groups and hydrogens attached to bridging oxygen atoms are frozen. The lengths of all bonds including hydrogen atoms are constrained to their equilibrium values. Electrostatic interactions are calculated by the pppm method with a precision of 10^{-5}. A 12.0 Å cutoff for the nonbonded interactions and for the real-space contribution of the electrostatics has been chosen. The production simulations are performed in an NVT ensemble using a Nosé−Hoover thermostat[34] with a time step of 2.0 fs at a temperature of 300 K. The height of the simulation cell is initially adjusted to maintain the standard water density in a volume element far away from the surface.

RESULTS AND DISCUSSION

Free Energy of Adsorption. Before discussing the adhesion mechanisms in detail, we first focus on quantifying the equilibrium adsorption in terms of a free energy driving force ΔG_{ads}. The general consistency between adsorption isotherms and microscopically calculated single molecule adsorption free energies has recently been shown in ref 35. For the minTBP-1 peptide, ΔG_{ads} can be estimated from the experimentally measured Langmuir dissociation constant K_L^{-1} = 13.2 ± 4.0 μmol/L, measured on Ti for the titanium binding peptide (TPB) RKLPDAPGMHTW[9] by employing the relationship[36,37]

$$\Delta G_{ads} = -k_B T \ln[c_{solv}/K_L^{-1}] = -0.394 \text{ eV} \quad (1)$$

where c_{solv} is the solvent concentration (55.5 mol/L for water). Compared to minTBP-1, TBP features an excess sequence of amino acids, which, however, has been shown to have no influence on the adsorption behavior of the molecule.[8] Therefore, in the absence of direct experimental information, we assume that the dissociation constant for the larger peptide can be used also to approximate the dissociation constant and, thus, estimate the ΔG_{ads} value, for the RKLPDA peptide adsorbing on Ti.

In ref 38 the free energy landscape of a peptide molecule in solution has been calculated using a combination of metadynamics and replica exchange molecular dynamics (REMD). As we will proceed to show in the following, a converged profile of the adsorption free energy of the peptide projected along the z coordinate perpendicular to the surface can be computed in a similar manner: We employ well-tempered metadynamics[39,40] to explore the reaction coordinate combined with replica exchange with solute tempering (REST)[41] to enhance sampling of the peptide's phase space. In detail, Gaussian hills with a height of 0.03 eV and a width of 0.1 Å are deposited every 0.5 ps. The simulations are performed in the well-tempered ensemble[40] with a bias factor of 10.0. Four replicas at solute temperatures of 300, 350, 400, and 450 K are employed, and exchanges between replicas are attempted every picosecond (further technical details about these simulations are given in the Supporting Information).

The trajectory of the reaction coordinate and the evolution of the bias potential with simulation time are shown in Figure 1.

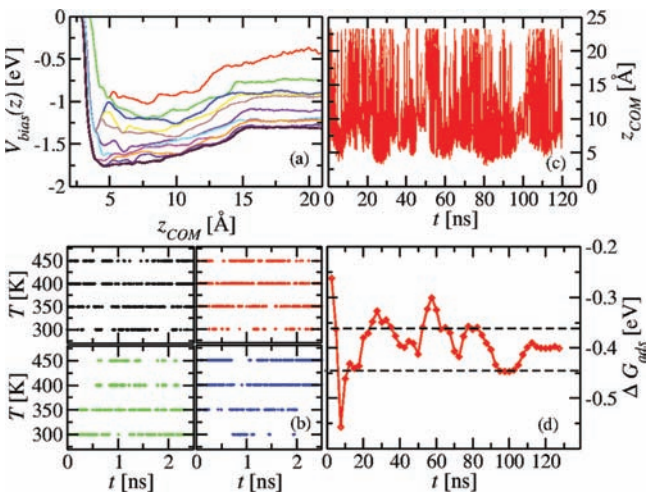

Figure 1. Details of the metadynamics+REST simulation to obtain the adsorption free energy of the minTBP-1 on titanium: (a) time evolution of the bias potential; (b) section of the trajectories of the four replicas in temperature space; (c) trajectory of the reaction coordinate; (d) time evolution of the integrated ΔG_{ads} value. The dashed line marks the estimated error bars.

As displayed in Figure 1b, all replicas are able to access the entire temperature range, even on a time scale of nanoseconds, which is the prerequisite for effective sampling. Moreover, at the base temperature the reaction coordinate exhibits a large number of transitions between adsorbed states and bulk solution (Figure 1c), a requirement for equilibrium conditions.

dx.doi.org/10.1021/ja210744g | J. Am. Chem.Soc. 2012, 134, 2407−2413

From the free energy profile, we can compute a net free energy of adsorption ΔG_{ads} as[42]

$$\Delta G_{ads} = -k_B T \ln \frac{c_{ads}}{c_{bulk}} \quad (2)$$

where

$$c_{ads} = \frac{1}{z_0 - z_{min}} \int_{z_{min}}^{z_0} \exp(-\beta G(z))\, dz$$

$$c_{bulk} = \frac{1}{z_{max} - z_0} \int_{z_0}^{z_{max}} \exp(-\beta G(z))\, dz$$

and z_0 defines the border between the adsorbed region and the bulk solution (set to 15.0 Å in this case, as indicated by the dashed line in Figure 2). Figure 1d displays the evolution of

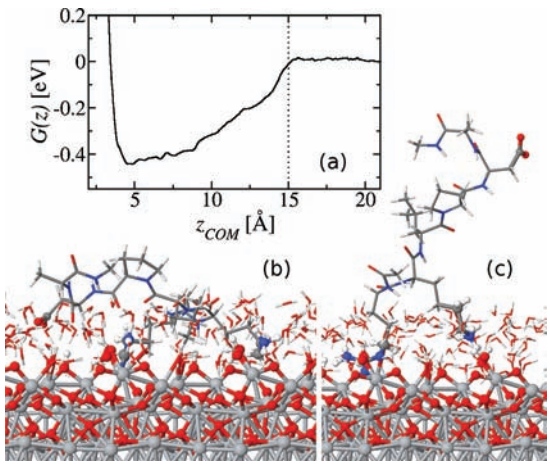

Figure 2. Free energy profile of the RKLPDA peptide on the oxidized titanium surface obtained by metadynamics+REST (a). Typical adsorbed peptide structures: flat (b) and upright conformation (c).

ΔG_{ads} with increasing simulation time. After about 50 ns, the free energy difference merely oscillates around the final value without further systematic change. From the amplitude of these oscillations, we estimate the error as 0.04 eV.

The final profile after 120 ns of simulation is displayed in Figure 2. The integrated value of the adsorption free energy amounts to $\Delta G_{ads} = -0.40 \pm 0.04$ eV, which is in excellent agreement with the experimental reference.

In the region close to the free energy minimum, we identify two main adsorbed geometries: (i) a flat, tightly bound geometry where the R, K, and D side chains are close to the surface (Figure 2b); (ii) a more upright geometry more where surface contact is established merely through the positively charged end group of R (in most cases accompanied by K), while the carboxylate group of D remains in solution (Figure 2c).

Adhesion Forces. To compute adhesion forces and compare our results to the AFM force spectroscopy experiments of refs 10 and 11, we perform a series of steered molecular dynamics simulations (SMD)[43] as described in ref 24. Similar to the experiments, we employ the oxidized silicon surface as a reference material in these simulations. To gather a representative statistical sampling, special attention was paid to the generation of 29 independent adsorption conformations for titanium and 31 conformations for silicon (for the details, see the Supporting Information). On Ti, these initial geometries reflect the same adsorption behavior as obtained from our metadynamics+REST simulations. On the Si surface we find a similar adsorption mode, in which the R residue always remains close to the surface, in most cases accompanied by the K side chain. In contrast to Ti, though, we rarely observe attachment of the aspartic acid residue to the surface.

For each adsorbed configuration, the molecule is pulled off the surface using a time-dependent harmonic potential

$$V_{smd}(z_c, t) = \frac{1}{2} k_{smd}(z_c - z_0(t))^2 \quad (3)$$

where the z-coordinate z_C of the carbon atom of the NME cap at the C-terminal end of the peptide is tethered to an anchor $z_0(t) = z_C(t = 0) + v_{smd}t$ moving with constant velocity. Each simulation is carried out until the molecule completely desorbs from the surface (up to 7 ns in each case), with parameters k_{smd} = 0.5 eV/Å^2 and v_{smd} = 0.5 m/s, which we have found to yield reasonable force profiles while allowing a sufficiently large number of individual simulations (see Supporting Information, Figure S5).

The force−displacement curves typically exhibit an initial increase of the force and feature several smaller subpeaks until a maximum peak is reached, after which the force decays rapidly (see inset of Figure 3). The maximum peak forces obtained in

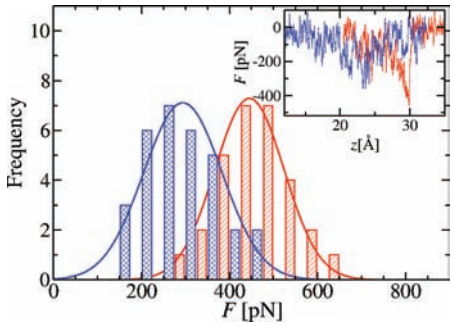

Figure 3. Histograms of the SMD force peaks and typical force-displacement curves (displayed in the inset) on titanium (red) and on silicon (blue).

each SMD run are displayed as a histogram in Figure 3. They range from 250 to 650 pN for the Ti surface and from 150 to 500 pN for Si. Average detachment forces are obtained by fitting the histograms with Gaussian functions, yielding 445 ± 79 pN on titanium and 294 ± 89 pN on silicon. These force values are about a factor 3 smaller than those of the AFM experiments of refs 10 and 11. This is most probably due to the fact that the experiments were performed with RKLPDA-modified ferritin proteins, meaning that the measured forces likely contain contributions from more than one peptide and from ferritin itself. Moreover, owing to the high pulling velocity in our simulations, a quantitative comparison of the *absolute force values* to experiments is problematic. We note, however, that the experimental force distribution measured on Ti in the presence of TWEEN20 surfactant,[10,44] introduced to reduce hydrophobic protein−surface interactions and obtain values representative of a single RKLPDA peptide, agrees remarkably well with our simulation results (the measured average force on Ti is 500 ± 160 pN). More importantly, our test simulations show that the velocity dependence of the adhesion forces on both substrates is almost the same (see Supporting Information, Figure S5), which allows us to quantify *the ratio*

dx.doi.org/10.1021/ja210744g | J. Am. Chem.Soc. 2012, 134, 2407−2413

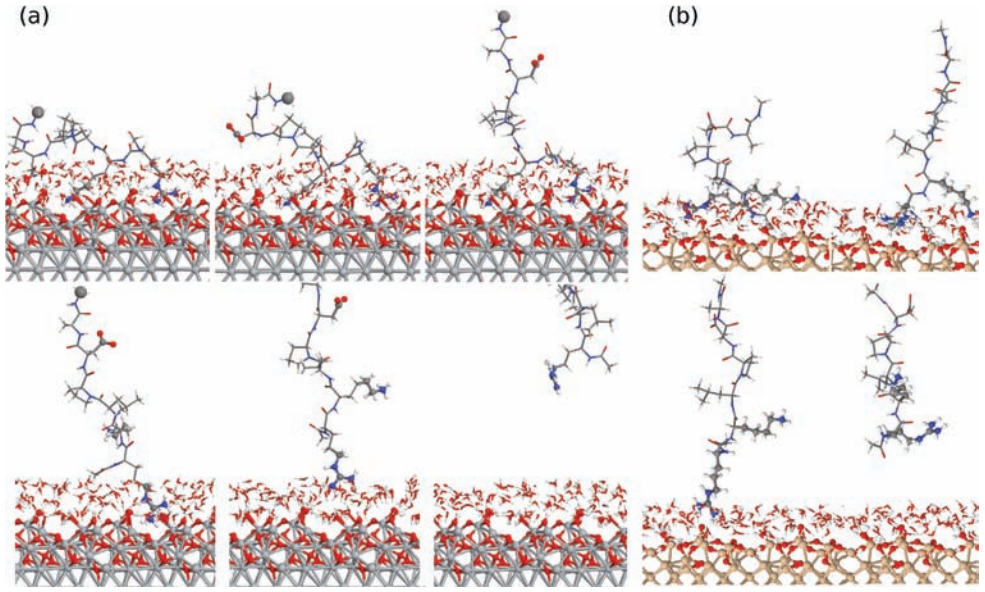

Figure 4. Snapshot of the trajectory of a typical SMD simulation of the RKLPDA peptide on the oxidized titanium (a) and silicon (b) surfaces.

between the average adhesion forces on the two surfaces in a reliable way, assuming that the detachment mechanisms are not affected by the pulling speed. The ratio between Ti and Si obtained in our simulations is about 1.5, which is in excellent agreement with the experimental ratio of about 1.6 obtained experimentally in pure water.[11]

Analysis of SMD. The general agreement of our simulation results with experimental data, including both macroscopic (ΔG_{ads}) and microscopic (F_{SMD}) observables, encourages us to carefully analyze the trajectories of the SMD simulations in order to elucidate the mechanisms underlying the specific adhesion. Irrespective of the initial conditions, on Ti the maximum force peaks are associated with the detachment of either the R or the K side chain, whereas detachment of the D residue causes merely a smaller prepeak of about 250 pN (see Figures 4 and 5). In part, this is due to the fact that K and R are naturally the last residues to be pulled off the surface when the harmonic spring is attached to the alanine C-terminal of the peptide, consistent with the AFM experimental setup. However, the consistently smaller force values associated with detachment of D indicate an intrinsically weaker anchoring via this residue. Similarly, on Si the maximum desorption forces are associated with the detachment of either the R (as shown as a typical example in Figure 5) or the K side chains, although the force peaks generally emerge less distinctly than on Ti.

The similar desorption behavior on Ti and Si argues against a significant influence of the chemical nature of the adsorbed residues on the different adhesion forces. As proposed by Hayashi et al.,[10,11] the D residue indeed exhibits a higher affinity for Ti than for Si. However, our simulations reveal that the different behavior of D influences just the *equilibrium adsorption mode* and not the *maximum adhesion forces*, as they involve exclusively the detachment of R and K. Instead, the major differences between Ti and Si seem to arise from the specific interactions of the latter side chains with the markedly different structures of the water solvent at the solid/liquid interfaces and, thus, from the degree of surface hydrophilicity.

Water Structures on the Two Surfaces. The density profiles of water oxygen atoms along the normal direction to the Ti and Si surfaces are displayed in Figure 6, revealing the

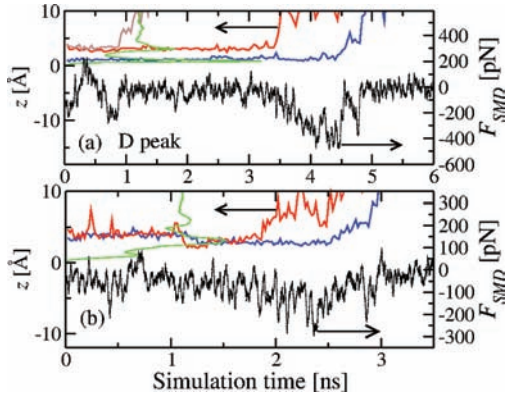

Figure 5. Trajectories of the central C atom of the R end group (blue) and of the N atom of K (red) along with the corresponding SMD forces (black) on titanium (a) and silicon (b) and the respective water density profile (green). Additionally, on Ti the carboxylate C of the D residue is displayed (brown).

expected, pronounced layering of the water molecules in both cases. On titanium, however, the density within the first layer is much larger, the layer width is smaller, and even the second layer still emerges distinctly, being comparable to the first main peak on silicon. This evident structuring is intriguing, given that both surface models exhibit considerable topological roughness and chemical heterogeneity. In fact, a laterally resolved analysis of the water structure reveals that on the Ti surface the density maxima appear as localized spots, whereas on Si they assume a rather continuous form. In addition, the Si surface presents evident patches of reduced water density, which can be associated with local hydrophobic sites, as found on silica and quartz surfaces in previous works.[35,45] Interestingly, the adsorption geometry of the peptide is directly influenced by the local density changes in the water structure, resulting in subtle differences in the adsorption configurations of the R and K side chains on Ti or Si, as shown in Figure 6. On Si the aliphatic parts of the side chains spread almost flat within regions of low water density, while the charged moieties occupy high-density positions. On Ti the side chains adsorb in a more upright manner, suggesting a stronger hydrophilic character of

dx.doi.org/10.1021/ja210744g | J. Am. Chem.Soc. 2012, 134, 2407−2413

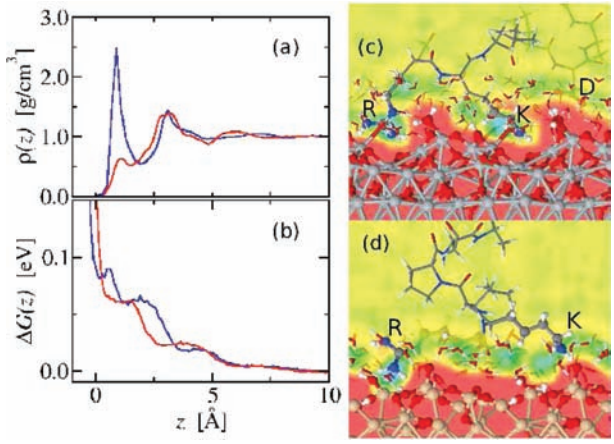

Figure 6. (a) Density profile of water oxygen on Ti (blue) and on Si (red). (b) The free energy profiles of a spherical hydrophobic solute on Ti (blue) and on Si (red). (c, d) Adsorbed peptide on Ti and Si, respectively, with a map of the unperturbed water density (displayed within a vertical plane, which includes the R and K end groups).

the surface. In particular, localized water density maxima, resulting from the atomic-scale surface roughness of the oxidized surface, act as adsorption "hot spots", stably anchoring the polar R and K end groups during the SMD simulations until detachment.

A quantitative assessment of the hydrophilic character of the two surfaces is performed by calculating the adsorption free energy[46] of a spherical hydrophobic solute of radius 2.5 Å. Its interactions with all other atoms are modeled by a WCA potential,[47] following the method introduced in refs 48 and 49. As displayed in the inset of Figure 6, the computed adsorption free energy profile is positive in both cases, indicating hydrophilic surfaces. The stepwise increase of the free energy profile bears the signature of the water layers, which successively have to be penetrated upon approaching the surface. Though differences between both surfaces are subtle, particularly the height of the last step in proximity of the surface is larger on Ti compared to Si, suggesting a more stable water structure and hence a slightly stronger hydrophilic character.

Different Forces from Different Water Structures. Considering in detail the *z*-trajectory (Figure 5) of the guanidinium group of R and the ammonium group of K on the Ti surface, we find that the latter preferentially resides within the first or the second water layer, where it forms hydrogen bonds with surface hydroxyl groups, adsorbed water molecules, and bridging oxygen atoms. The former always accommodates reproducibly in a tilted position within the first water layer where it can interact directly with the surface atoms underneath and, at the same time, form a network of hydrogen bonds with both the solvent and the adsorbed water and hydroxyl groups (cf. Figure 6). The anchoring of R within the first layer of adsorbed water constitutes a significant difference of the natively oxidized Ti to the TiO_2 rutile 110 surface, where the first layer of water is tightly bound to the 5-fold coordinated titanium atoms and can hardly be entered by other adsorbates.[50]

On the Si surface both the R and the K side chains reside within the first, broad water layer, seeking proximity of a silanol or silanoate group to establish hydrogen bonds, while direct interaction with surface bridging oxygen atoms is rarely observed. Due to the lesser extent of structuring within the first solvent layer, when the peptide is pulled off the surface, the force increases up to a less pronounced maximum peak and does not drop sharply afterward, indicating a softer desorption transition compared to the Ti surface (see Figure 5).

Adsorption of the End Groups. The effects of the specific interfacial solvent structure on the driving force for peptide adsorption are quantifed by metadynamics[51] calculations of the free energy adsorption profiles for isolated R, K, and D side chains, modeled by a $CNHCH_3(NH_2)_2^+$, a $CH_3NH_3^+$, and a CH_3COO^- molecule, respectively (Figure 7). The acetate molecule presents only a very shallow minimum in proximity of

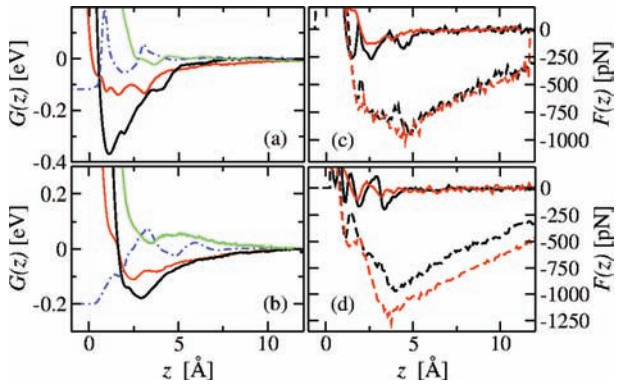

Figure 7. Free energy profiles for truncated arginine (black), lysine (red) and aspartic acid (green) side chains on titanium (a) and silicon (b). The respective water density profiles (in arbitrary units) are depicted by the dotted blue lines. Full (solid lines) and dry (dashed lines) equilibrium forces acting on the arginine (c) and the lysine (d) side chains, respectively, on titanium (black) and silicon (red).

the Ti and a local minimum in proximity of the Si surface. This is separated from the bulk by a free energy barrier, explaining the absence of D adsorption in our simulations of the RKLPDA peptide on Si. For K and R the adsorption takes place barrierlessly into well-defined energy minima. Using eq 2, the strongest adsorption free energy ΔG_{ads} is computed for R on Ti, amounting to −0.31 eV compared to −0.15 eV on Si. For K, we compute weaker binding energy values of −0.09 eV on Ti and −0.07 eV on Si.

We note that the adsorption behavior of the side chains observed in the simulations of the whole peptide is recovered from these profiles. On Ti, R adsorbs stably in the first water layer with metastable states between both layers and inside the second layer, whereas K is most stably located within the second layer, with local minima in the first layer accessible upon overcoming a small free energy barrier. On Si, the most favorable position of both residues is within the first, broad water layer. Remarkably, the methyl-ammonium molecule analogous to the K residue can approach the Si surface via both the polar ammonium end and the nonpolar methyl group, in line with simulation results for methanol on quartz surfaces.[45] This indicates once more the presence of mixed hydrophobic/hydrophilic regions close to each other on oxidized Si, which has significant implications on the adsorption behavior of polypeptides. The overall shape of the free energy profiles reflects well the water density structure, with the density maxima coinciding with the free energy minima (see also Supporting Information, Figure S4) and with the more or less sharp structure of the water peaks corresponding with more or less pronounced slopes of the free energy wells. In particular, as the adhesion forces are determined by the free energy slopes,

dx.doi.org/10.1021/ja210744g | J. Am. Chem.Soc. 2012, 134, 2407−2413

higher forces are expected for the Ti surface, in agreement with the results of the SMD simulations presented above (see Figure 3).

A careful analysis of the metadynamics simulations allows us now to assess the influence of the water structure on the surface adhesion. For each molecule and surface, we can compute force profiles $F(z)$ along the adsorption trajectories by taking into account either all interactions ("wet" forces) or only direct molecule−surface interactions ("dry" forces), as displayed in Figure 7. The most evident result from this analysis is that the dry forces are much larger and much longer-ranged than the wet forces, due to the absence of electrostatic screening by the orientational and structural ordering of the water molecules above the surface and by the counterions. Remarkable is the inversion of the interaction strength; that is, the dry adsorption forces are larger on the *silicon* surface. Instead, the wet forces on *titanium* clearly exceed the corresponding values on silicon, consistently with the results of our SMD simulations of the whole RKLPDA peptide.

Importantly, the peaks of the force profile not only can be assigned to the transitions between metastable states in the free energy profile but also correspond to the peaks of the water density profile. In particular, we find multiple distinct force peaks for adsorption at the Ti/water interface and only a single broad force peak for adsorption at the Si/water interface. In contrast, the dry forces lack a clear structure, again suggesting that adhesion forces are largely mediated by the water structure at the interface, which is thus at the origin of the stronger interactions with the Ti surface.

CONCLUSIONS

In summary, our results provide a clear rationalization of the origin of the specific titanium recognition by the RKLPDA peptide. Consistently with the results of alanine substitution experiments,[9,11] the R residue is mainly responsible for the stable anchoring of the peptide to the surface. In addition, we have found that the positively charged K and, in part, also the negatively charged D residues contribute to the equilibrium adsorption on Ti. The presence of D on the surface generally causes a flat, tightly bound conformation; otherwise, the molecule assumes a more upright adsorption geometry. From metadynamics+REST simulations we have found these adsorbed conformations to be associated with an adsorption free energy of −0.40 eV, in quantitative agreement with experimental data. This is remarkable given the simplicity of our force-field approach, which has been parametrized by means of first-principles reference data obtained only for a limited amount of surface−molecule interactions,[24] and relies on the assumption that pairwise additive interactions are sufficiently accurate to describe liquid water in contact with TiO_2 or SiO_2 surfaces.

In extensive SMD simulations we have computed an average detachment force on Ti 1.5 times higher than that on Si, in good agreement with AFM experiments. Our simulations reveal that only R and K contribute significantly to the maximum adhesion forces on *both* materials. This finding contradicts the experimental hypothesis that different adhesion forces result from an electrostatically driven selectivity of the surfaces toward specific residues. Instead, by means of accurate calculations of adsorption free energy profiles, we have found a striking correlation between the adhesion forces and the nanoscale features of the water structuring at the solid/liquid interfaces. In fact, the interfacial water structuring has been found in previous studies to govern, for instance, the adhesion between silicon wafers[21] or the adsorption mode of a collagen fragment on hydrophobic surfaces.[52] A novel, crucial finding of this study is that the local solvent density variations near a heterogeneous, rough surface are sensed by the side chains of a peptide in a way that bears many features characteristic of the specific recognition in biomolecular aggregates. Our simulation highlights the importance not only of direct surface−molecule interactions at the anchoring points but also of an alternation between hydrophilic and hydrophobic residues to optimize the matching with the solvent density oscillations. In this picture, electrostatic interactions still play an important role in driving the approach of charged residues toward surfaces with opposite charge density, but they are, at least in this case, of secondary importance as far as adhesion forces are concerned. We anticipate that accurate experimental investigations of the adhesion forces and free energies of oligopeptides with carefully designed sequences on oxidized surfaces presenting a controlled degree of hydrophobicity/hydrophilicity, fabricated, for example, by plasma deposition techniques varying the precursors composition, may give further support of the theoretical predictions formulated in our work.

ASSOCIATED CONTENT

Supporting Information

Details regarding the force field parameters, the simulation protocols, and the convergence of the free energy and adhesion force calculations. This material is available free of charge via the Internet at http://pubs.acs.org.

AUTHOR INFORMATION

Corresponding Author

colombi@hmi.uni-bremen.de

ACKNOWLEDGMENTS

We are indebted to Tiffany Walsh for useful suggestions and critical reading of the draft manuscript. We acknowledge funding from the Deutsche Forschungsgemeinschaft (DFG) under the Emmy Noether grant CI 144/2 and from the EU-FP7-NMP grant 229205 "ADGLASS". Computer time was allocated at the HLRN (Hannover-Berlin) and the ZIH (Dresden) supercomputing centers.

REFERENCES

(1) Sarikaya, M.; Tamerler, C.; Jen, A. K.-Y.; Schulten, K.; Baneyx, F. *Nat. Mater.* **2003**, *2*, 577−585.
(2) Shiba, K. *Curr. Opin. Biotechnol.* **2010**, *21*, 412−425.
(3) Peelle, B. R.; Krauland, E. M.; Wittrup, K. D.; Belcher, A. M. *Langmuir* **2005**, *21*, 6929−6933.
(4) Di Felice, R.; Corni, S. *J. Phys. Chem. Lett.* **2011**, *2*, 1510−1519.
(5) Herbers, C. R.; Johnston, K.; van der Vegt, N. F. A. *Phys. Chem. Chem. Phys.* **2011**, *13*, 10577−10583.
(6) Ghiringhelli, L. M.; Hess, B.; van der Vegt, N. F. A.; Site, L. D. *J. Am. Chem. Soc.* **2008**, *130*, 13460−13464.
(7) Schravendijk, P.; Ghiringhelli, L. M.; Site, L. D.; van der Vegt, N. F. A. *J. Phys. Chem. C* **2007**, *111*, 2631−2642.
(8) Sano, K.-I.; Shiba, K. *J. Am. Chem. Soc.* **2003**, *125*, 14234−14235.
(9) Sano, K.-I.; Sasaki, H.; Shiba, K. *Langmuir* **2005**, *21*, 3090−3095.
(10) Hayashi, T.; Sano, K.-I.; Shiba, K.; Kumashiro, Y.; Iwahori, K.; Yamashita, I.; Hara, M. *Nano Lett.* **2006**, *6*, 515−519.
(11) Hayashi, T.; Sano, K.-I.; Shiba, K.; Iwahori, K.; Yamashita, I.; Hara, M. *Langmuir* **2009**, *25*, 10901−10906.
(12) Skelton, A. A.; Liang, T.; Walsh, T. R. *ACS Appl. Mater. Interface* **2009**, *1*, 1482−1491.

(13) Tamerler, C.; Sarikaya, M. *Philos. Trans. R. Soc. A* **2009**, *367*, 1705−1726.
(14) Khoo, X.; Hamilton, P.; O'Toole, G. A.; Snyder, B. D.; Kenan, D. J.; Grinstaff, M. W. *J. Am. Chem. Soc.* **2009**, *131*, 10992−10997.
(15) Kokubun, K.; Kashiwagi, K.; Yoshinari, M.; Inoue, T.; Shiba, K. *Biomacromolecules* **2008**, *9*, 3098−3105.
(16) Xiao, S.-J.; Textor, M.; Spencer, N. D. *Langmuir* **2998**, *14*, 5507−5516.
(17) Rammelt, S.; Illert, T.; Bierbaum, S.; Scharnweber, D.; Zwipp, H.; Schneiders, W. *Biomaterials* **2006**, *27*, 5561−5571.
(18) Raynor, J. E.; Petrie, T. A.; Fears, K. P.; Latour, R. A.; García, A. J.; Collard, D. M. *Biomacromolecules* **2009**, *10*, 748−755.
(19) Fang, Y.; Poulsen, N.; Dickerson, M. B.; Cai, Y.; Jones, S. E.; Naik, R. R.; Kroger, N.; Sandhage, K. H. *J. Mater. Chem.* **2008**, *18*, 3871−3875.
(20) Colombi Ciacchi, L.; Payne, M. C. *Phys. Rev. Lett.* **2005**, *96*, 196101−196104.
(21) Cole, D. J.; Csányi, G.; Payne, M. C.; Spearing, S. M.; Colombi Ciacchi, L. *J. Chem. Phys.* **2007**, *127*, 204704−204715.
(22) Colombi Ciacchi, L.; Cole, D. J.; Payne, M. C.; Gumbsch, P. *J. Phys. Chem. C* **2008**, *112*, 12077−12080.
(23) Schneider, J.; Colombi Ciacchi, L. *Surf. Sci.* **2010**, *604*, 1105−1115.
(24) Schneider, J.; Colombi Ciacchi, L. *J. Chem. Theory Comput.* **2011**, *7*, 473−484.
(25) Born, R.; Scharnweber, D.; Rößler, S.; Stölzel, M.; Thieme, M.; Wolf, C.; Worch, H. *Fresenius J. Anal. Chem.* **1998**, *361*, 697−700.
(26) Kosmulski, M. *Adv. Colloid Interface Sci.* **2002**, *99*, 255−264.
(27) McCafferty, E.; Wightman, J. P.; Cromer, T. F. *J. Electrochem. Soc.* **1999**, *146*, 2849−2852.
(28) Takahashi, K.; Fukuzaki, S. *Biocontrol Sci.* **2008**, *13*, 9−16.
(29) Hozumi, A.; Sugimura, H.; Yokogawa, Y.; Kameyama, T.; Takai, O. *Colloid Surf., A: Physicochem. Eng. Aspects* **182**, *2001*, 257−261.
(30) Tadros, T. F.; Lyklema, J. *J. Electroanal. Chem.* **1968**, *17*, 267−275.
(31) Cornell, W. D.; Cieplak, P.; Bayly, C. I.; Gould, I. R.; Merz, K. M. Jr.; Ferguson, D. M.; Spellmeyer, D. C.; Fox, T.; Caldwell, J. W.; Kollman, P. A. *J. Am. Chem. Soc.* **1995**, *117*, 5179−5197.
(32) Plimpton, S. J. *J. Comput. Phys.* **1995**, *117*, 1−19.
(33) Jorgensen, W. L.; Chandrasekhar, J.; Madura, J. D.; Impey, R. W.; Klein, M. L. *J. Chem. Phys.* **1983**, *79*, 926−935.
(34) Hoover, W. G. *Phys. Rev. A* **1985**, *31*, 1695−1697.
(35) Carr, R.; Comer, J.; Ginsberg, M. D.; Aksimentiev, A. *J. Phys. Chem. Lett.* **2011**, *2*, 1804−1807.
(36) Serro, A. P.; Degianpietro, K.; Colaco, R.; Saramago, B. *Colloids Surf., B* **2010**, *78*, 1−7.
(37) Dringen, R.; Koehler, Y.; Derr, L.; Tomba, G.; Schmidt, M. M.; Treccani, L.; Ciacchi, L. C.; Rezwan, K. *Langmuir* **2011**, *27*, 9449−9457.
(38) Bussi, G.; Gervasio, F. L.; Laio, A.; Parrinello, M. *J. Am. Chem. Soc.* **2006**, *128*, 13435−13441.
(39) Laio, A.; Gervasio, F. L. *Rep. Prog. Phys.* **2008**, *71*, 126601−126622.
(40) Barducci, A.; Bussi, G.; Parrinello, M. *Phys. Rev. Lett.* **2008**, *100*, 020603−020606.
(41) Liu, P.; Kim, B.; Friesner, R. A.; Berne, B. J. *Proc. Natl. Acad. Sci. U.S.A.* **2005**, *102*, 13749−13754.
(42) O'Brien, C. P.; Stuart, S. J.; Bruce, D. A.; Latour, R. A. *Langmuir* **2008**, *24*, 14115−14124.
(43) Isralewitz, B.; Gao, M.; Schulten, K. *Curr. Opin. Struct. Biol.* **2001**, *11*, 224−230.
(44) Yamashita, I.; Kirimura, H.; Okuda, M.; Nishio, K.; Sano, K.-I.; Shiba, K.; Hayashi, T.; Hara, M.; Mishima, Y. *Small* **2006**, *2*, 1148−1152.
(45) Notman, R.; Walsh, T. R. *Langmuir* **2009**, *25*, 1638−1644.
(46) The PMF of the hydrophibicWCA solute is calculated by performing an equilibrium simulation without bias potential for 20 ns. The free energy is evaluated using the probability ratio method, $G(\lambda) = -kBT \ln P(\lambda)$, which we have found to yield equivalent results compared to other approaches involving a bias potential.
(47) Weeks, J.; Chandler, D.; Andersen, H. *J. Chem. Phys.* **1971**, *54*, 5237−5247.
(48) Godawat, R.; Jamadagni, S. N.; Garde, S. *Proc. Natl. Acad. Sci. U.S.A.* **2009**, *106*, 15119−15124.
(49) Acharya, H.; Vembanur, S.; Jamadagni, S. N.; Garde, S. *Faraday Discuss.* **2010**, *146*, 353−365.
(50) Monti, S.; Walsh, T. R. *J. Phys. Chem. C* **2010**, *114*, 22197−22206.
(51) We choose the *z*-coordinates of the central C atom in R, the N atom in K, and the C atom in D as reaction coordinate. We deposit Gaussian hills with 0.02 eV height and 0.1 Å width every 0.4 ps. Convergence is achieved by employing the well-tempered ensemble with a bias factor of 5.0.
(52) Cole, D. J.; Payne, M. C.; Ciacchi, L. C. *Phys. Chem. Chem. Phys.* **2009**, *11*, 11395−11399.